Radiative transfer of elastic waves versus finite difference simulations in two-dimensional random media

J. Przybilla,[1] M. Korn,[1] and U. Wegler[1]

Received 21 July 2005; revised 14 December 2005; accepted 12 January 2006; published 19 April 2006.

[1] High-frequency seismograms mainly consist of incoherently scattered waves. Although their phases are more or less random, their envelopes show smooth and stable variations depending on frequency and distance. Envelope modeling can thus be used to infer stochastic parameters of the heterogeneous Earth medium. Radiative transfer theory (RTT) describes energy transport through a random heterogeneous medium neglecting phase information and has been frequently used to simulate observed mean square (MS) envelopes of high-frequency waves. The radiative transfer equations can be numerically solved by Monte Carlo simulations. So far, mostly isotropic scattering and acoustic approximations have been used. Here we present an extension of the Monte Carlo method to the full elastic case including *P*, *S*, and conversion scattering where the single scattering events are described by angular-dependent scattering coefficients in random media which follow from the Born approximation. In order to validate the method, the simulated envelopes are compared to average envelopes obtained by full waveform modeling with a finite difference method in two-dimensional random media with Gaussian and exponential correlation functions. Envelope shapes agree remarkably well for both short and long lapse times and for a broad range of scattering parameters. We conclude that the use of Born scattering coefficients in RTT does not pose severe limits on its validity range. Even in the strong forward scattering regime, envelope broadening and peak amplitude delays can be successfully modeled if one includes the wandering effect as obtained from the parabolic wave equation and Markov approximation into RTT.

Citation: Przybilla, J., M. Korn, and U. Wegler (2006), Radiative transfer of elastic waves versus finite difference simulations in two-dimensional random media, *J. Geophys. Res.*, *111*, B04305, doi:10.1029/2005JB003952.

1. Introduction

[2] High-frequency wave propagation through the inhomogeneous Earth medium is an extremely complex process. The wavefield emitted from a source is strongly deformed by the scattering process at small-scale random heterogeneous structure. Seismograms at distant receivers exhibit long-lasting and highly variable wave trains usually called coda waves [*Aki*, 1969; *Aki and Chouet*, 1975]. The phase of coda waves is more or less random, but their envelopes show a much simpler behavior with smooth variations depending on distance and frequency. Therefore it has become common practice to use envelopes instead of complete waveforms to gain an understanding of the heterogeneous structure and the statistical characteristics of the propagation medium. Amplitude attenuation, peak delay, envelope broadening, and coda decay rate are some of the parameters that can be deduced from observed envelope shapes [e.g., *Scherbaum and Sato*, 1991; *Gusev and Abubakirov*, 1999]. There have been a number of approaches to model envelope shapes in media with random fluctuations of the elastic parameters. Among them are single-scattering Born theory [*Sato*, 1977], mean wave theory [*Müller and Shapiro*, 2001], energy flux model [*Frankel and Wennerberg*, 1987; *Korn*, 1993], and diffusion theory [*Dainty and Toksöz*, 1977; *Margerin et al.*, 1998; *Trègourés and van Tiggelen*, 2002; *Wegler*, 2004]. More recently, the Markov approximation has become popular [*Williamson*, 1972; *Sato and Fehler*, 1998; *Saito et al.*, 2002; *Korn and Sato*, 2005]. It is based on the acoustic parabolic wave equation and is useful to model envelope broadening and peak delay in the time window near the direct wave onset in the case of strong forward scattering, but neglects large angle and conversion scattering. Its accuracy has been proved by comparison with finite difference methods [*Saito et al.*, 2003; *Korn and Sato*, 2005]. Radiative transfer theory (RTT) on the other hand [*Wu*, 1985; *Gusev and Abubakirov*, 1987; *Hoshiba*, 1991; *Zeng et al.*, 1991; *Apresyan and Kravtsov*, 1996] describes energy transport through a scattering medium neglecting phase

[1]Institut für Geophysik und Geologie, Universität Leipzig, Leipzig, Germany.

0148-0227/06/2005JB003952$09.00

information. It can be strictly derived from the elastic wave equation [*Rytov et al.*, 1987; *Weaver*, 1990; *Ryzhik et al.*, 1996] and is, in principle, capable of modeling both short and long lapse time coda. Thus it is more general than Markov theory which is only valid for short lapse times and diffusion theory which is valid for long lapse times and/or strong scattering. RTT works well if typical scale length of the heterogeneities and wavelength are of comparable size, and if medium fluctuations are moderate. Analytical solutions to the radiative transfer equation exist for the case of isotropic scattering in acoustic [*Zeng et al.*, 1991; *Paasschens*, 1997] and elastic media [*Zeng*, 1993]. For more complex cases numerical solutions employing Monte Carlo (MC) methods have been employed.

[3] In seismology MC was first proposed by *Gusev and Abubakirov* [1987]. *Yoshimoto* [2000] developed a MC scheme for scattering of acoustic waves in randomly fluctuating media superimposed on a depth-dependent background velocity. Later *Margerin et al.* [2000] solved the RTT equation for elastic waves including conversion scattering and anisotropic scattering at isolated identical scatterers. *Shearer and Earle* [2004] presented numerical examples for short-period wave scattering in the mantle. Here we formulate MC solutions to the elastic wave RTT equation in two dimensions and compare them to average mean square (MS) envelopes obtained from finite difference simulations of complete wavefields in single realizations of random media with Gaussian and exponential autocorrelation functions. In the acoustic case a comparison between FD and RTT simulations was done by *Wegler et al.* [2006]. Restriction to two dimensions is due to the fact that large-scale three-dimensional (3-D) finite difference computations are still cumbersome even on today's computers. Our MC approach is based on the well-known Born single-scattering coefficients and includes conversion scattering and angular-dependent scattering. It is generally expected that Born approximation breaks down in the regime of strong forward scattering. Therefore *Sato et al.* [2004] had proposed a hybrid method for envelope synthesis combining RTT for large angle scattering and Markov approximation for forward scattering. Our comparisons show, however, that the validity range of RTT using Born scattering coefficients extends much further into the forward scattering regime than expected, and that the breakdown of RTT occurs in a predictable manner. Therefore our version of RTT will be capable of accurately synthesizing complete envelopes from the first *P* arrival until the late coda for most practical applications.

2. Elastic Radiative Transfer Equation

[4] The radiative transfer equation was introduced phenomenologically in astrophysics to describe energy transport of light through the atmosphere [*Chandrasekhar*, 1960]. Only later, a strict derivation from the wave equation was achieved [*Rytov et al.*, 1987; *Ryzhik et al.*, 1996; *Weaver*, 1990]. *Wu* [1985] and *Hoshiba* [1991] introduced the RTT into seismology to explain the generation of the seismic coda by seismic wave scattering at the heterogeneous structure of the Earth. Usually isotropic scattering of acoustic waves is simulated. The vector nature of elastic waves and the conversions between *P* and *S* waves are neglected. Here we use the elastic RTT in 2-D which can be written as

$$\begin{aligned}
\frac{1}{\alpha_0}\frac{\partial I^p}{\partial t} + \hat{\mathbf{k}}\cdot\nabla I^p &= \frac{1}{2\pi}\int g_{pp}(\hat{\mathbf{k}},\hat{\mathbf{k}}')I^p(\hat{\mathbf{k}}')d\hat{\mathbf{k}}' \\
&\quad - g^0_{pp}I^p + \frac{1}{2\pi}\int g_{sp}(\hat{\mathbf{k}},\hat{\mathbf{k}}')I^s(\hat{\mathbf{k}})d\hat{\mathbf{k}}' - g^0_{ps}I^p \\
\frac{1}{\beta_0}\frac{\partial I^s}{\partial t} + \hat{\mathbf{k}}\cdot\nabla I^s &= \frac{1}{2\pi}\int g_{ss}(\hat{\mathbf{k}},\hat{\mathbf{k}}')I^s(\hat{\mathbf{k}}')d\hat{\mathbf{k}}' \\
&\quad - g^0_{ss}I^s + \frac{1}{2\pi}\int g_{ps}(\hat{\mathbf{k}},\hat{\mathbf{k}}')I^p(\hat{\mathbf{k}}')d\hat{\mathbf{k}}' - g^0_{sp}I^s;
\end{aligned} \tag{1}$$

see *Ryzhik et al.* [1996] for the 3-D reference. Here $I^p = I^p(t, \mathbf{x}, \hat{\mathbf{k}})$ and $I^s = I^s(t, \mathbf{x}, \hat{\mathbf{k}})$ are the specific intensities of *P* and *S* waves, respectively. Unit wave numbers $\hat{\mathbf{k}}'$ and $\hat{\mathbf{k}}$ denote incidence and scattered wave directions. Mean velocities are α_0 and β_0 for *P* and *S* waves. (The ∇ is an abbreviation for two-dimensional gradient operator $(\partial/\partial x, \partial/\partial y)$). The left-hand sides of the coupled equations describe the intensity transport of *P* and *S* modes and represent the total time derivative of intensities. The right-hand sides describe the influence of scattering through the angular-dependent scattering coefficients $g_{ij}(\hat{\mathbf{k}}, \hat{\mathbf{k}}')$ and the total scattering coefficients g^0_{ij}. This is a sum of loss and gain terms, loss outward from the direction of propagation and gain from all directions into the direction of propagation. Coupling between both equations is given by conversion scattering coefficients g_{ps} and g_{sp}. The RTT equation can be derived from the Bethe-Salpeter equation using the so called ladder approximation with the validity range $(ka\varepsilon)^2 \ll 1$ [*Rytov et al.*, 1987, p.151]. For a complete derivation of RTT from the wave equation we refer to *Ryzhik et al.* [1996].

[5] The basic assumptions for the validity of RTT can be expressed as follows: (1) scattering is weak, (2) wavelength and scale length of the heterogeneities are of comparable size, and (3) phases of waves from different scatterers are independent of each other, i.e., the energy of scattered wave packets can be stacked. Numerical solutions can be obtained by Monte Carlo methods. In the acoustic case this was done, e.g., by *Gusev and Abubakirov* [1987], *Hoshiba* [1991], *Hoshiba* [1995], and *Yoshimoto* [2000]. For vector RTT equations, see *Bal and Moscoso* [2000] and *Margerin et al.* [2000].

2.1. Random Medium

[6] A random medium can be described by velocity and density fluctuations around a background mean value. We write the velocity as

$$V(\mathbf{x}) = V_0 + \delta V(\mathbf{x}) = V_0(1 + \xi(\mathbf{x})), \tag{2}$$

where $\xi(\mathbf{x})$ is the fluctuation of wave velocity and

$$V_0 = \langle V(\mathbf{x})\rangle \qquad \langle \xi(\mathbf{x})\rangle = 0. \tag{3}$$

The autocorrelation function (ACF) is defined as ensemble mean value

$$R(\mathbf{y}) = \langle \xi(\mathbf{x})\xi(\mathbf{x}+\mathbf{y})\rangle, \tag{4}$$

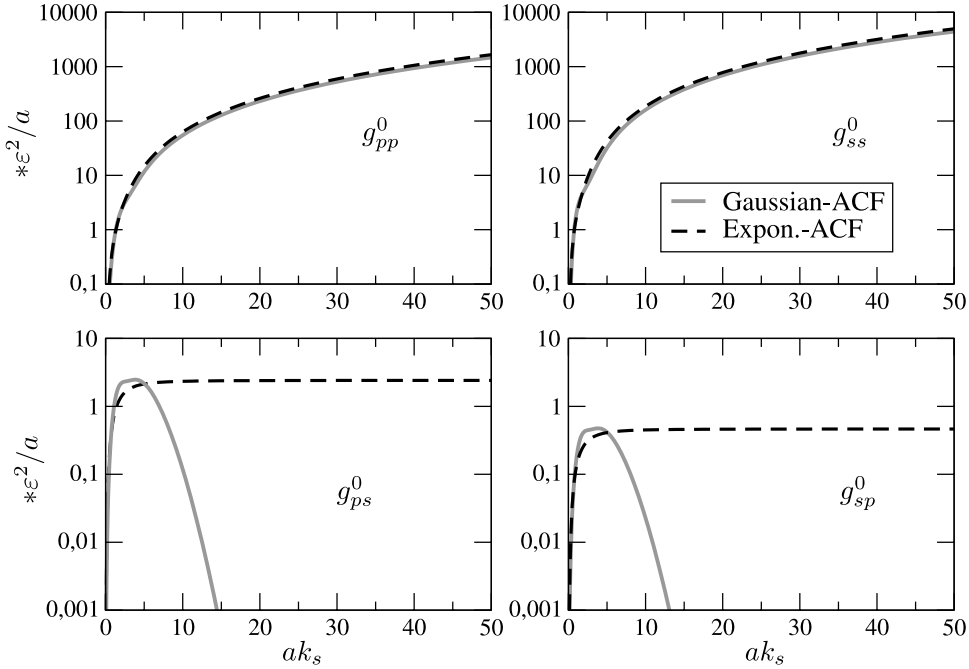

Figure 1. Total scattering coefficients for Gaussian (gray lines) and exponential (dashed black lines) ACF. Conversion scattering coefficients g^0_{ps} and g^0_{sp} vanish for large values of $a\ k_s$ for Gaussian ACF but are constant for exponential ACF; k_s is S wave number.

with variance

$$\varepsilon^2 = R(0) = \langle \xi(\mathbf{x})^2 \rangle. \tag{5}$$

In this paper we use the 2-D Gaussian and exponential ACF Gaussian

$$R_G(\mathbf{x}) = R_G(r) = \varepsilon^2 \exp\left(-r^2/a^2\right) \tag{6}$$

Exponential

$$R_E(\mathbf{x}) = R_E(r) = \varepsilon^2 \exp(-r/a), \tag{7}$$

with $r = |\mathbf{x}|$ and correlation distance a. The power spectra of the random media are

$$P_G(m) = \pi a^2 \varepsilon^2 \exp\left(-a^2 m^2/4\right) \tag{8}$$

$$P_E(m) = \frac{4\pi\varepsilon^2 a^2}{(1 + a^2 m^2)^{3/2}}. \tag{9}$$

To reduce the number of independent medium parameters, we chose correlated velocity and density fluctuations from Birch's law [*Birch*, 1961]:

$$\frac{\delta\alpha}{\alpha_0} = \frac{\delta\beta}{\beta_0} = \nu\frac{\delta\rho}{\rho_0}, \tag{10}$$

where α_0, β_0 are P and S wave mean velocities, ρ is density and $\nu = 0.8$ [*Sato and Fehler*, 1998].

2.2. Elastic Born Scattering Coefficients

[7] For the scattering coefficients in equation (1), we use the single scattering coefficients obtained from Born approximation [*Wu and Aki*, 1985; *Sato and Fehler*, 1998]. In two dimensions they read

$$g_{pp}(\theta) = \frac{\gamma_0 k_s^3}{8\pi} P\left(\frac{2k_s}{\gamma_0}\sin(\theta/2)\right)|X_r^{pp}|^2, \tag{11}$$

$$g_{ps}(\theta) = \frac{k_s^3}{8\pi} P\left(\frac{k_s}{\gamma_0}\sqrt{1 + \gamma_0^2 - 2\gamma_0\cos\theta}\right)|X_\theta^{ps}|^2, \tag{12}$$

$$g_{sp}(\theta) = \frac{\gamma_0 k_s^3}{8\pi} P\left(\frac{k_s}{\gamma_0}\sqrt{1 + \gamma_0^2 - 2\gamma_0\cos\theta}\right)|X_r^{sp}|^2, \tag{13}$$

$$g_{ss}(\theta) = \frac{k_s^3}{8\pi} P(2k_s\sin(\theta/2))|X_\theta^{ss}|^2. \tag{14}$$

Here the argument of the power spectrum P is the absolute value of exchange wave number $|\vec{k}^{\,\mathbf{scatt}}_{\mathbf{p,s}} - \vec{k}^{\,\mathbf{inc}}_{\mathbf{p,s}}|$ between scattered and incident wave and θ is the scattering angle. We use $k_p = k_s/\gamma_0$ with $\gamma_0 = \alpha_0/\beta_0$. Quantities

$$X_r^{pp} = \frac{1}{\gamma_0^2}\left[\nu\left(-1 + \cos\theta + \frac{2}{\gamma_0^2}\sin^2\theta\right) - 2 + \frac{4}{\gamma_0^2}\sin^2\theta\right] \tag{15}$$

$$X_\theta^{ps} = \sin\theta\left[\nu\left(-1 + \frac{2}{\gamma_0}\cos\theta\right) + \frac{4}{\gamma_0}\cos\theta\right] \tag{16}$$

$$X_r^{sp} = -\frac{1}{\gamma_0^2}X_\theta^{ps} \tag{17}$$

$$X_\theta^{ss} = (\nu(\cos\theta - \cos 2\theta) - 2\cos 2\theta) \tag{18}$$

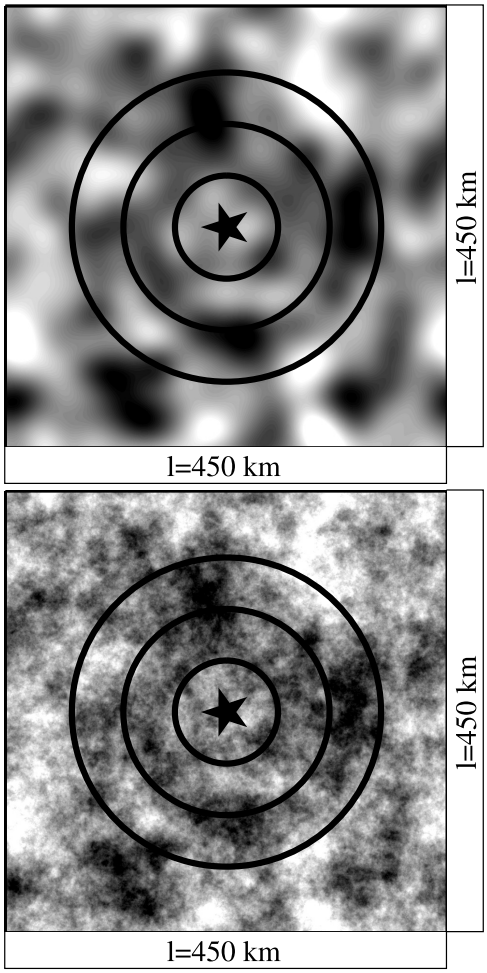

Figure 2. Model representation for (top) Gaussian and (bottom) exponential random medium. The receivers are placed long circles at 50, 100, and 150 km distance.

are the scattering patterns, which only depend on scattering angle. The total scattering coefficients are obtained as mean values of all scattering directions by integrating the scattering coefficients over θ:

$$g_{kj}^0 = \frac{1}{2\pi} \oint g_{kj} d\theta. \tag{19}$$

Indices k and j are p and s, respectively. Figure 1 shows the dependence of the total scattering coefficients on parameters ε^2/a and dimensionless wave number ak_s. The coefficients scale linearly with ε^2/a. Coefficients g_{pp}^0 und g_{ss}^0 behave similar for all values of ak_s, but conversion scattering coefficients g_{ps}^0 und g_{sp}^0 differ between exponential and Gaussian ACF. In the Gaussian case, g_{ps}^0 and g_{sp}^0 vanish for large values of ak_s, but for exponential ACF they are constant. This means that for large values of ak_s, no conversion between P and S waves takes place in the Born approximation for Gaussian ACF. We return to this point later.

3. Elastic MC Simulations

[8] It is common practice to solve the RTT equation by a Monte Carlo method. Energy transport is described by wave packets or particles emitted from the source into arbitrary directions θ and moving with constant velocity until they experience a scattering event. The distance s between two scattering events is given by the exponential distribution For P waves

$$s_p = -l_p \ln \gamma \tag{20}$$

For S waves

$$s_s = -l_s \ln \gamma, \tag{21}$$

with a uniformly distributed random number $\gamma \in (0, 1)$. Here indices p and s indicate P or S waves, l_p and l_s are the scattering mean free path lengths. They are related to the total scattering coefficients by

$$l_p = \left(g_{pp}^0 + g_{ps}^0\right)^{-1} \qquad l_s = \left(g_{ss}^0 + g_{sp}^0\right)^{-1}, \tag{22}$$

[9] We obtain the scattering mean free times t_p^* for P waves and t_s^* for S waves from the mean free path lengths by division through the velocities

$$t_p^* = l_p/v_p \qquad t_s^* = l_s/v_s. \tag{23}$$

Table 1. Simulation Parameters, Scattering Mean Free Paths, and Scattering Mean Free Times[a]

a, km	ε, %	l_p, km	t_p^*, s	l_s, km	t_s^*, s	$(k_s a\varepsilon)^2$
			Gaussian Medium			
1	2	304	51	168	16	5.3×10^{-3}
3.1	5	18	3	6	0.6	0.3
7.5	2	43	7	14	1	0.3
			Exponential Medium			
1	2	265	44	118	11	5.3×10^{-3}
3.1	5	15	2.5	5	0.5	0.3
16	5	3	0.5	1	0.1	8.4

[a]Parameters a and ε used for the numerical simulations, the scattering mean free paths l_p and l_s (equation (22)) and scattering mean free times t_s^* and t_p^* (equation (23)); the validity condition from the ladder approximation $(ka\varepsilon)^2 \ll 1$.

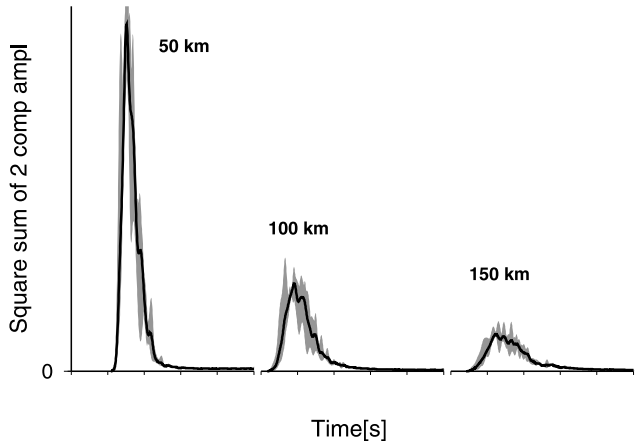

Figure 3. Ensemble averaged FD envelope for an exponential medium (a = 3.1 km, ε = 5%) (black line). The gray shaded area indicates the fluctuations of the MS envelopes for different realizations of the random medium.

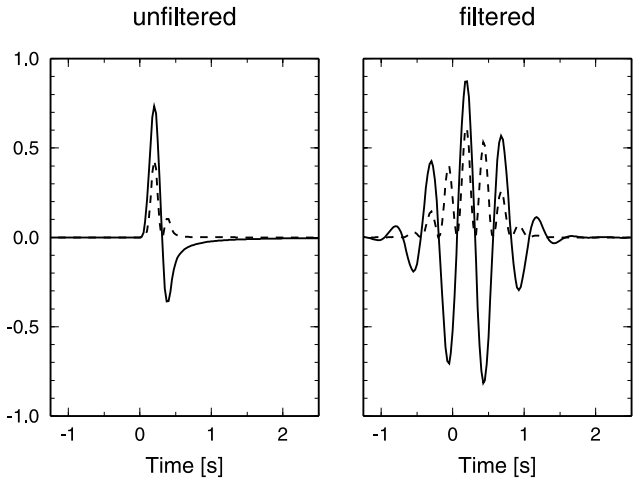

Figure 4. FD wavelet (solid line) and squared wavelet (dashed line) without and with an additional Gaussian band-pass filter (1.6 to 2.4 Hz).

For a P wave, the probability Π for P-to-P and P-to-S scattering is given by

$$\Pi(P \text{ to } P) = \frac{g^0_{pp}}{g^0_{pp} + g^0_{ps}}, \quad \Pi(P \text{ to } S) = 1 - \Pi(P \text{ to } P). \tag{24}$$

For a S wave the probabilities are

$$\Pi(S \text{ to } S) = \frac{g^0_{ss}}{g^0_{ss} + g^0_{sp}}, \quad \Pi(S \text{ to } P) = 1 - \Pi(S \text{ to } S). \tag{25}$$

After selecting the scattering mode we select the new propagation direction from the angular-dependent scattering coefficients through

$$1 - \gamma = \int_0^{\theta} \frac{g_{jk}(\theta')}{g^0_{jk}} d\theta' \tag{26}$$

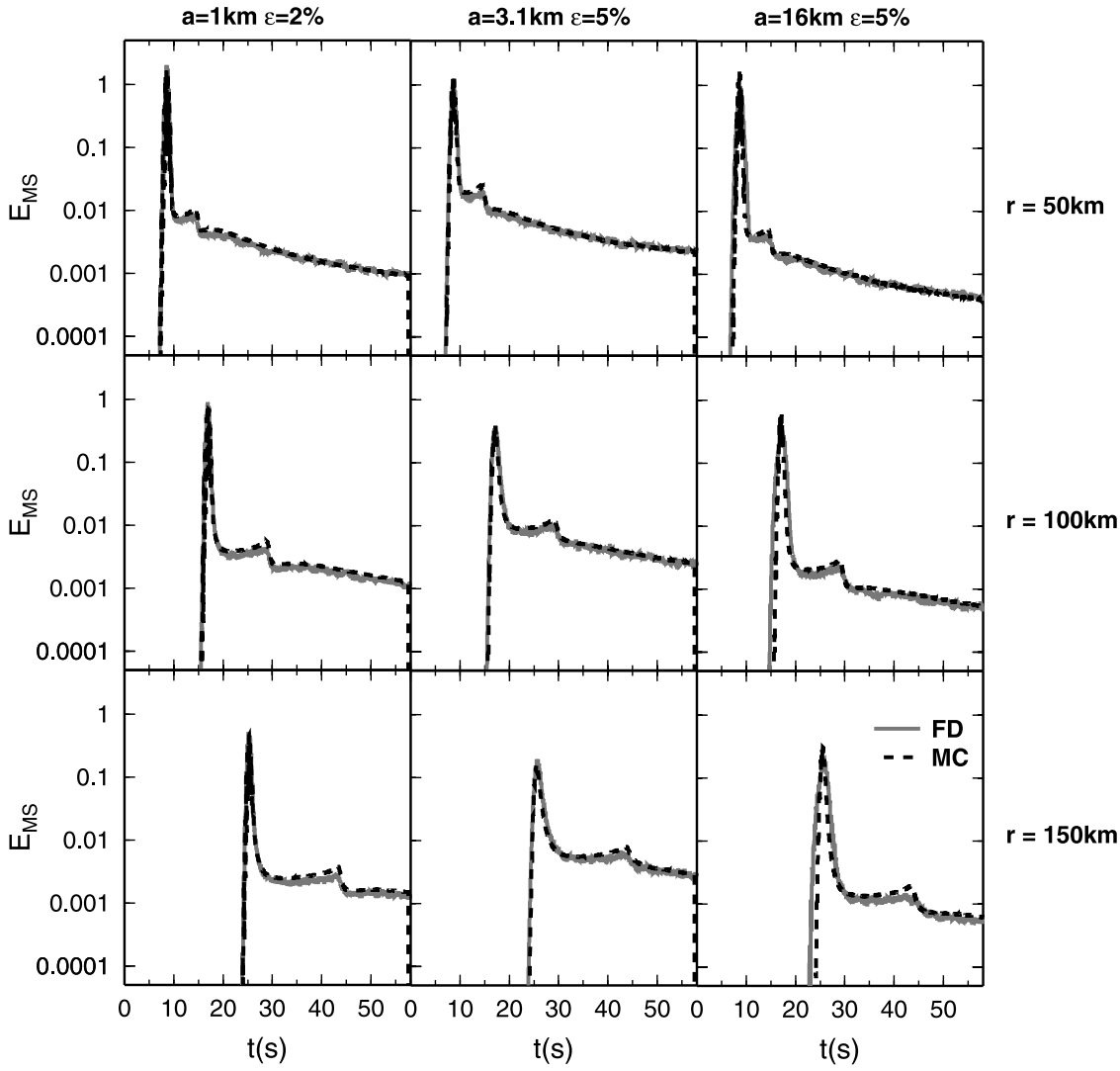

Figure 5. Comparison of MS envelopes for FD (solid gray) and MC (dashed black) simulations in an exponential medium for 3 combinations of correlation distance a and RMS fluctuations ε. The scattering mean free times are (left) $t_p^* = 44.2$ s, $t_s^* = 11.4$ s, (middle) $t_p^* = 2.5$ s, $t_s^* = 0.5$ s, and (right) $t_p^* = 0.5$ s, $t_s^* = 0.1$ s.

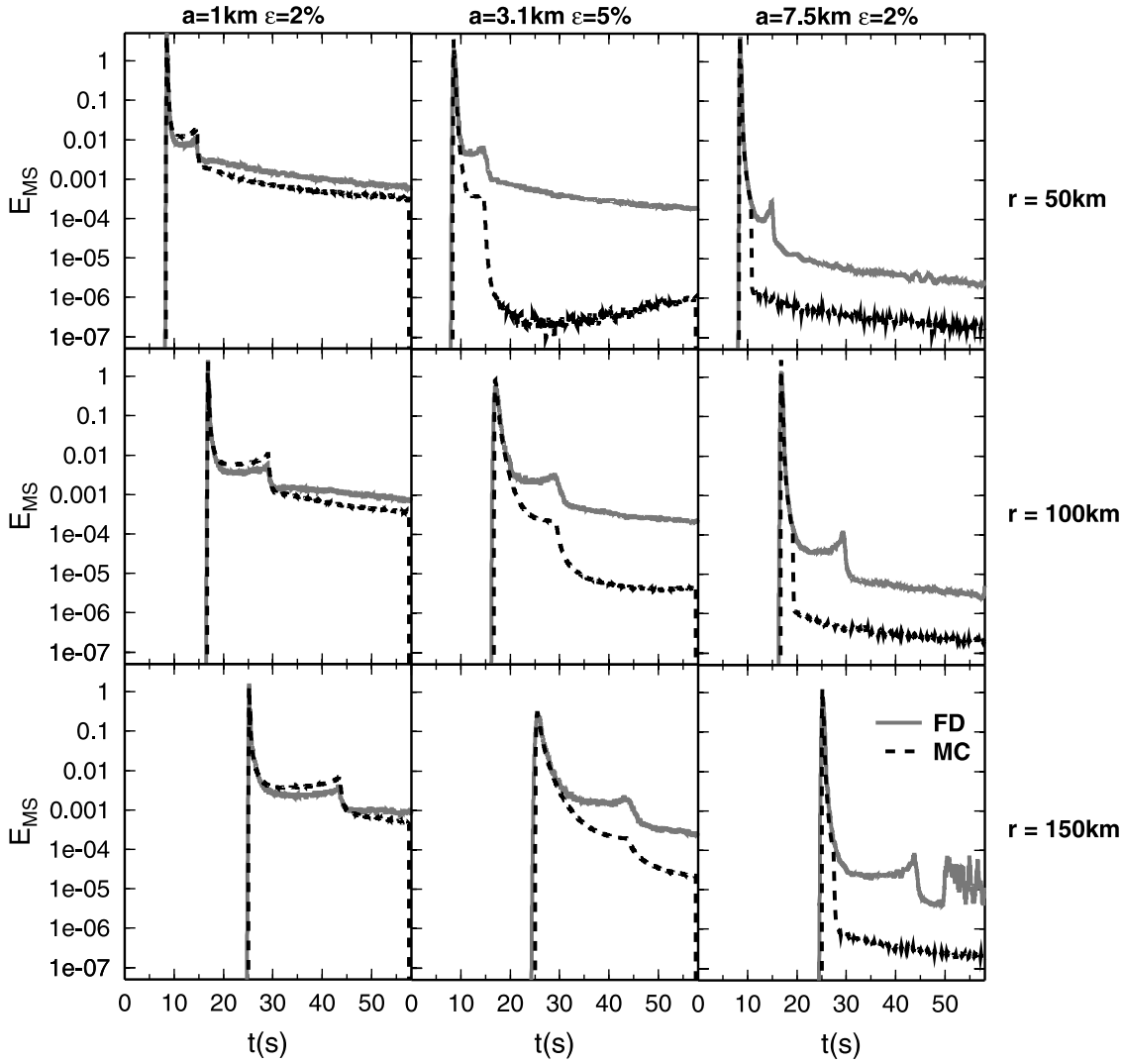

Figure 6. Same as Figure 5 for Gaussian ACF but with some of parameters a and ε different. The scattering mean free times are (left) $t_p^* = 50.7$ s, $t_s^* = 16.2$ s, (middle) $t_p^* = 3$ s, $t_s^* = 0.6$ s, and (right) $t_p^* = 7.2$ s, $t_s^* = 1.4$ s.

with an uniformly distributed random variable $\gamma \in (0, 1)$. Because there is usually no analytical solution to the integrals in equation (26), we perform a numerical integration and store it into tables. To obtain the MS envelope at receiver distance r, we count all particles that pass through a spherical shell of radius r and some thickness Δr in a small time step Δt as $N(r, t)$. The energy density which is proportional to MS envelope is then given by

$$E(r,t) = \frac{N(r,t)}{N_0 V(r)}, \tag{27}$$

where N_0 is the total number of particles and $V(r)$ is the receiver volume of the spherical shell. For more details of particle transport, see *Lux and Koblinger* [1991], and for a probabilistic theory of transport processes, see *Bal et al.* [2000].

4. Finite Difference Simulations in 2-D Elastic Media

[10] For the computation of theoretical waveforms of vector waves in various realizations of 2-D random media a standard finite difference technique in space-time domain is employed. We use a scheme where the equations for particle velocities and stresses in an isotropic inhomogeneous elastic medium are solved on a staggered grid [*Levander*, 1988]. The accuracy is second order in time and fourth order in space. The size of the model is 450 by 450 km (see Figure 2). Mean P and S velocities are $\alpha_0 = 6$ km/s, and $\beta_0 = 3.46$ km/s. A random fractional velocity fluctuation $\xi(\mathbf{x})$ with Gaussian or exponential ACF is imposed on P and S velocities. Parameter are RMS fractional fluctuation ε and correlation distance a. A point source is located at the center of the grid. It radiates pure P waves by applying radial stresses to the grid points surrounding the source. The time derivative of the source stress is given by

$$u_{in} = \sin\frac{\pi n t}{T} - \left(\frac{n}{n+2}\right)\sin\frac{\pi(n+2)t}{T} \quad 0 \le t \le T, \tag{28}$$

where T is the duration of the wavelet and n is a parameter indicating the number of maxima and minima. Here, we

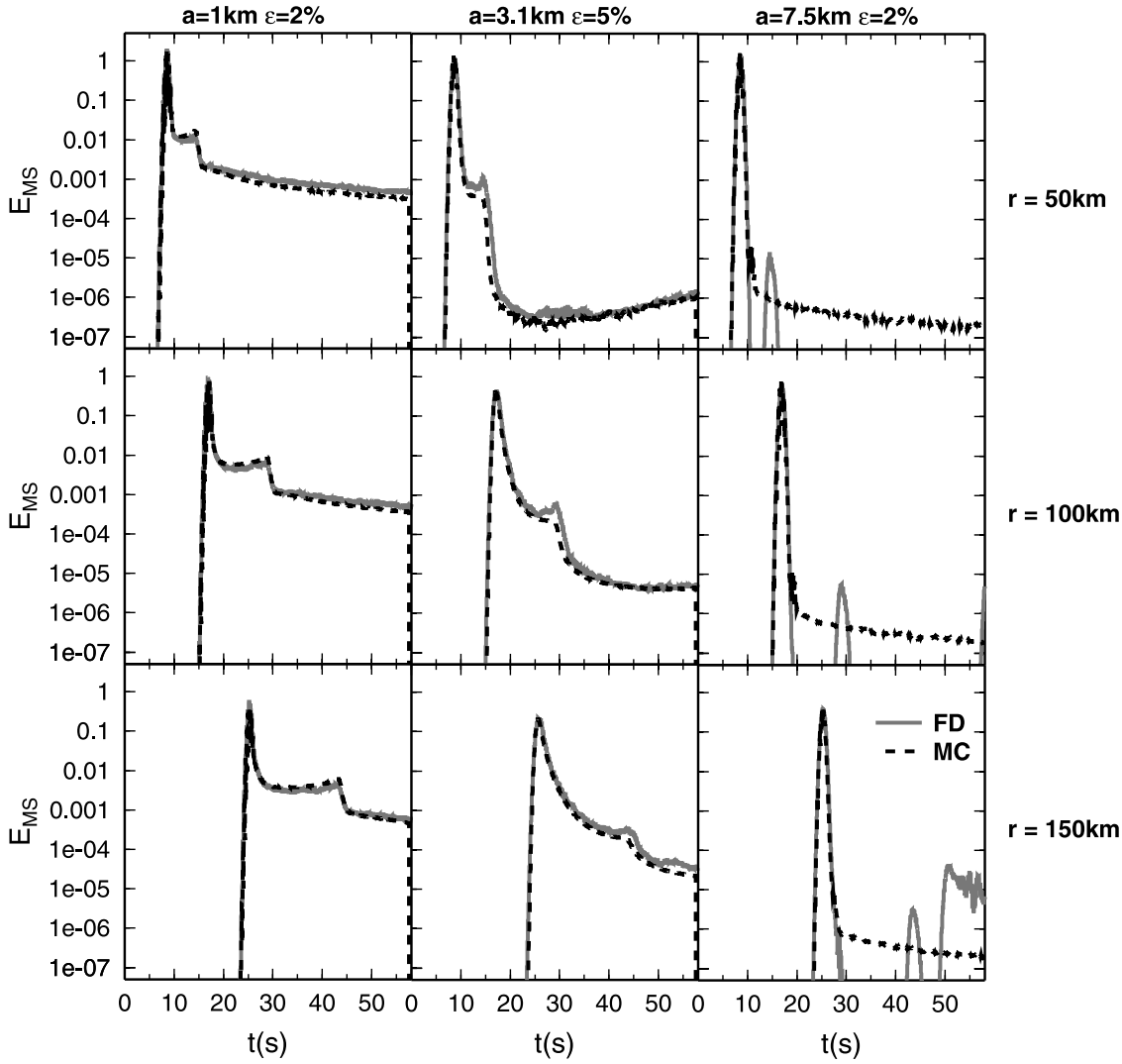

Figure 7. Same as Figure 6 with an additional band-pass filter applied to the FD traces. The increase of energy with time after the *S* onset at r = 50 km (middle) is an effect of strong forward scattering. Large angle scattering is small near the source for short times. The sag in the envelopes is only observable for small source receiver distances in a random medium which is poor on small-scale heterogeneities. The same effect is visible in the acoustic case [*Wegler et al.*, 2006]. We cannot see this effect on the right side for a = 7.5 km and ε = 0.02, because the level of coda energy is less.

choose n = 2 and T = 0.5 s to obtain a wavelet with dominant frequency of about 2 Hz and spectral half width between 0.8 and 4.1 Hz. Around the source a homogeneous region of 1 km width was introduced to ensure pure isotropic *P* wave radiation. The wavefield is recorded on circles at distances of 50, 100, and 150 km from the source. On each circle, 72 receivers are placed at azimuth increments of 5 degrees (see Figure 2). The spatial discretization in the FD scheme is 0.1 km, and the temporal discretization is 6 ms. This choice ensures that the numerical errors remain small. In a homogeneous medium with the mean velocities the phase velocity error introduced by grid dispersion would be 0.02% at the dominant frequency. At the boundaries of the computational grid absorbing boundary conditions are implemented. They are based on the paraxial approximation of the wave equation representing only the outgoing part of the wavefield. Here we use the boundary conditions suggested by *Reynolds* [1978] that are easy to implement into the staggered grid scheme. The presence of artificial boundaries introduce errors by generating weak spurious reflections and suppressing backward scattering from the area outside the grid. The grid size is chosen such that within the simulated time window only the receivers at 150 km are affected at times greater than 50 s. Numerical simulations have been performed for two values of RMS velocity fluctuation ε = 2% and ε = 5%, and for correlation distances ranging from 1 to 16 km. Thus the whole regime from weak forward scattering to strong forward scattering, has been covered (see Table 1). For each set of random parameters simulations for five different realization of the medium have been performed to obtain a sufficient ensemble averaging of the random wavefield. In Figure 3 the average MS envelope of all realizations for one set of parameters ε

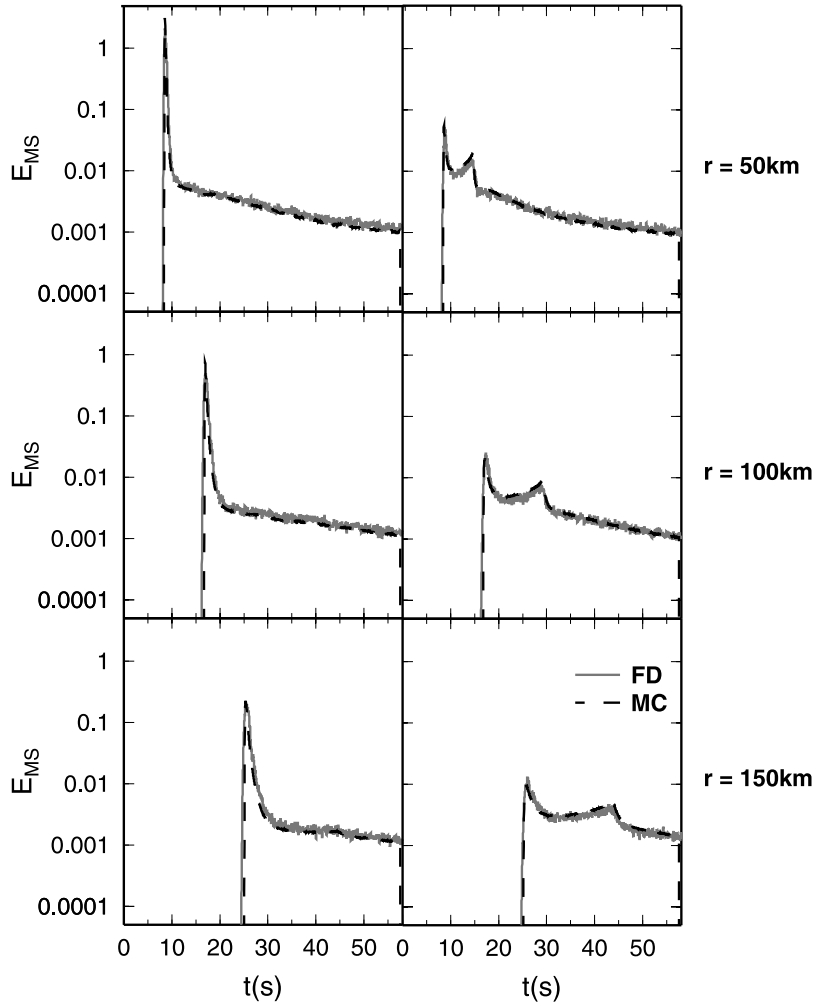

Figure 8. Comparison of radial and transversal components of energy density for exponential medium with a = 3.1 km, ε = 0.05.

and a is shown together with the maximum and minimum envelopes obtained from single realizations of the random medium. We only observe small amplitude fluctuations and conclude that our procedure provides a stable measure of the ensemble averaged MS envelopes.

[11] For the comparison with theoretical MS envelopes from the Monte Carlo simulation the following data processing was done: rotation of original components into radial and transverse components; stacking of the squared single-component traces of all receivers at fixed common distance and for all realizations; summing of radial and transverse squared components to obtain total MS envelopes. For some comparisons with the Monte Carlo envelopes an additional Gaussian bandpass filter was applied as the first processing step. There is one difference between the envelope shapes of the Monte Carlo and the FD simulations: In FD the outgoing wavelet has a pulse shape of finite length, whereas in the Monte Carlo method the particles are associated with a spike-like time function. In order to quantitatively compare both envelopes we convolved the Monte Carlo envelope with the squared FD wavelet. This wavelet is given as the convolution of the source time function (equation (4)) with an approximation to the 2-D far-field Greens function $g(t) = 1/\sqrt{t}$ and may be additionally bandpass filtered as above (Figure 4). Finally, FD and MC envelopes have been normalized by the time integral of the total envelope obtained at 50 km distance from the source in a homogeneous medium without scattering.

5. Comparison of Monte Carlo and FD Envelopes

5.1. Long Lapse Times

[12] Figure 5 shows the MS envelopes up to 60 s lapse time in logarithmic scale for exponential correlation function and correlation lengths between 1 and 16 km. Dimensionless wave number ak_s range from 2.1 to 33.5 for P waves. We find good agreement in the general coda level and decay rate for all cases, irrespective of the size of ak_s. We note that there is always a small peak in the coda at S wave arrival time, although no S waves are generated by the source. This peak obviously is caused by P-to-S conversions close to the source. Figure 6 shows the same for Gaussian correlation functions and correlation length a from 1 to 7.5 km. For larger parameter a the coda level is negligibly small. Coda level and decay rate do not agree between FD and MC except for the first arrival. Discrepancy becomes larger with increasing correlation distance. An explanation for this fact is that the total scattering coefficients g_{ps}^0 and g_{sp}^0

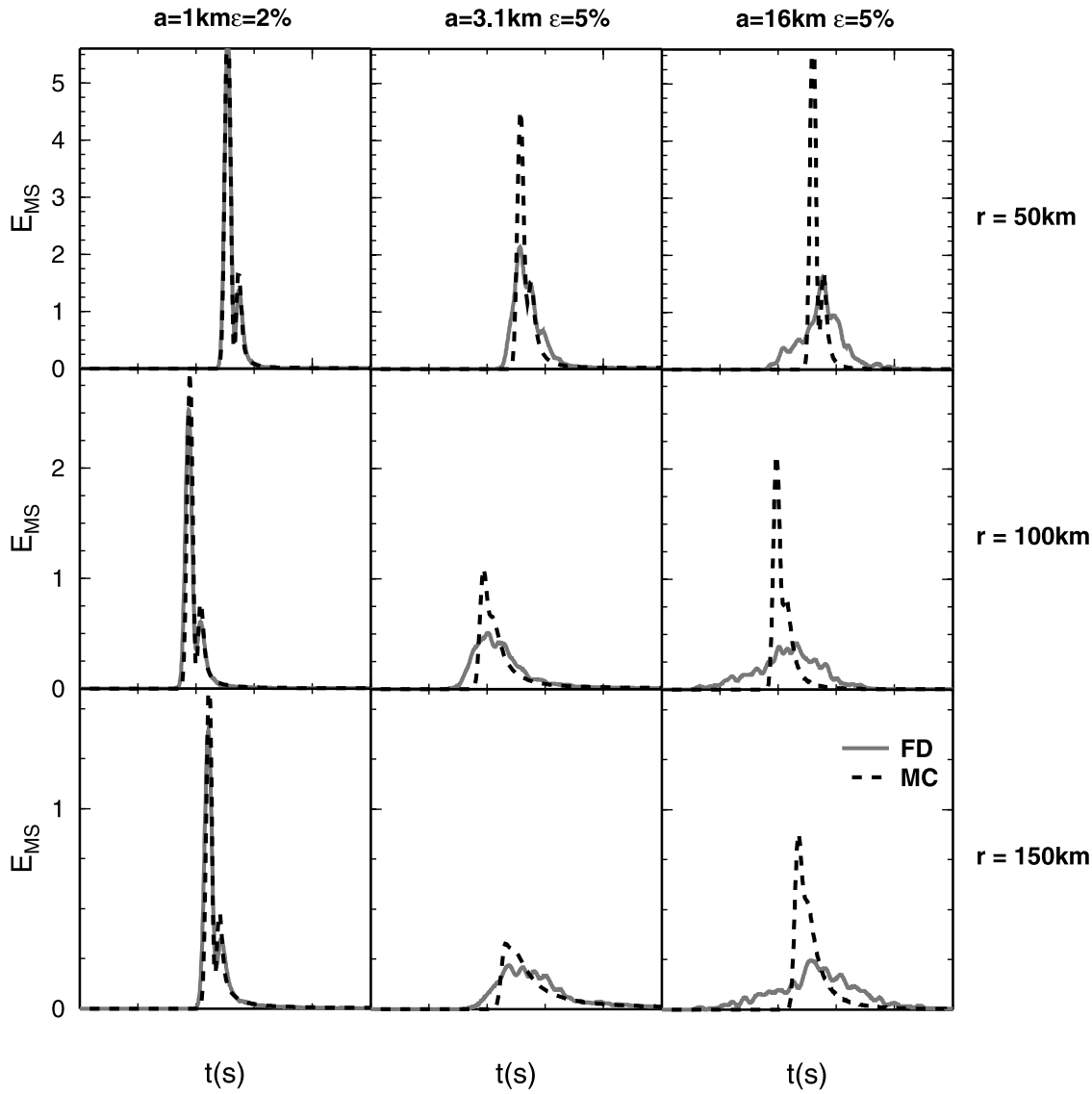

Figure 9. Close-up of MS envelope traces (FD and MC) for exponential medium around direct *P* arrival time, in linear scaling and different values of *a* and ε. Each tick mark on the *x* axis is 1 s in time. With increasing *a* the influence of traveltime fluctuations becomes more pronounced.

(see Figure 1) show a strong dependence on the parameter ak_s in the range considered here. This means that in Gaussian media a small change in frequency will greatly affect the conversion scattering. This effect is not present in exponential media. FD envelopes contain a range of frequencies according to the bandwidth of the source signal, whereas MC envelopes are strictly for one frequency only. We have applied an additional Gaussian bandpass filter to the FD traces which decreases the half width of the wavelet to 1.6–2.4 Hz. The effect of the filter on the shape of the effective source wavelet is shown in Figure 4. The MS envelopes of the filtered traces are shown in Figure 7. For a = 1 km and 3.1 km the FD and MC envelopes now agree with each other, except that the small peak at *S* wave arrival time is not present in the MC envelopes. For the large correlation distances, however, no agreement is found after the first arrival. The FD coda level is below the displayed range, but a peak at *S* wave arrival time is still clearly visible, whereas in MC a simple coda decay is found without any indication of forward scattered *S* waves. At r = 150 km the FD envelopes show some energy arriving after 50 s which is the reflection from the grid boundaries. Similar reflected energy is present in all simulations, but is at least one order of magnitude smaller than the coda energy in the exponential media. A possible explanation is that in Gaussian media the Born single scattering approximation in MC breaks down for large ak. The total Born scattering coefficients for conversion scattering g^0_{ps} and g^0_{sp} are effectively zero in this case, i.e., no conversion scattering can take place in MC. FD on the other hand has negligible coda amplitudes but still shows some *S* wave energy from conversion scattering near the source. This may be a consequence of near field scattering of the cylindrical wavefront, whereas in the Born approximation scattering of plane wavefronts is assumed. Figure 8 shows a comparison between FD and MC for radial and transverse component MS envelopes separately. The energy separation in components also agrees very well between both methods. It is clearly

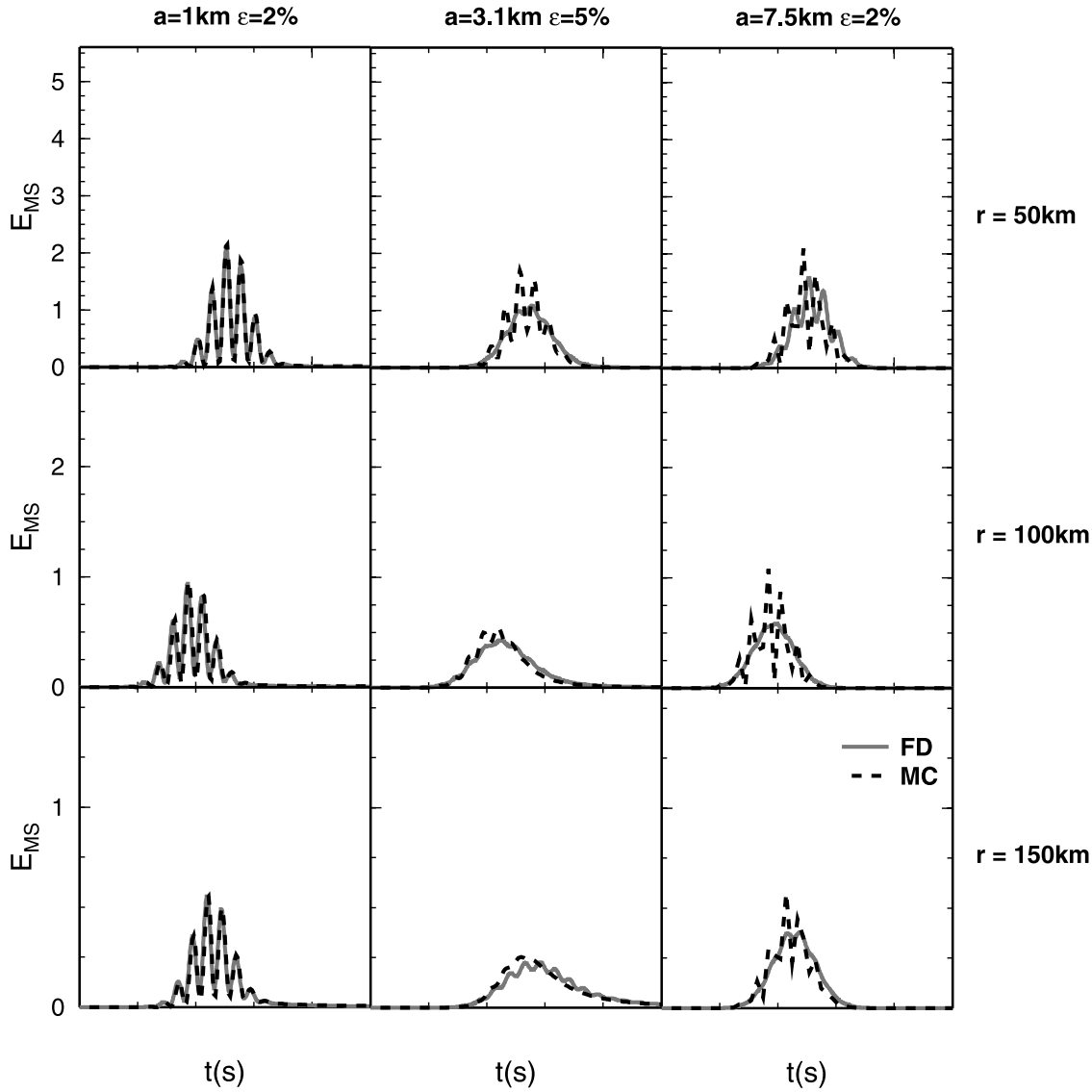

Figure 10. Same as Figure 9 but for a Gaussian medium with partly different values of a and ε. Band-pass-filtered traces have been used.

seen that at long lapse times both components carry about the same amount of energy. As can be expected the energy peak around S wave arrival time is only due to the transverse component, so that it can be interpreted as caused by forward scattered S waves generated by conversion scattering close to the source.

5.2. Short Lapse Times

[13] The pulse shape around the arrival time of the direct P wave is shown in detail in Figures 9 and 10 in linear scaling. The effective pulse shape is generated by small angle forward scattering. In the framework of Born approximation, strong forward scattering exists in the limit of large ak, and the effective pulse shape is given by the interference of multiply forward scattered waves. This makes the Monte Carlo solution rather cumbersome numerically because of short mean free path lengths. On the other hand, the question arises if radiative energy transfer neglecting phase differences between forward scattered particles remains valid at all. Figure 9 shows time windows around the arrival time of the P wave for different exponential media. For small correlation distance forward scattering is weak and the pulse shape essentially reproduces the squared wavelet (see Figure 4). At larger correlation distances small angle forward scattering becomes stronger and traveltime fluctuations become larger leading to broadening and collapsing of the FD pulse shapes. The MC envelopes also show some amount of broadening due to the delay of wave packets by small angle scattering, but they do not include the effect of statistical averaging of wave theoretical phase fluctuations along different paths through the random medium. This additional effect may be taken into account by considering the wandering effect [*Lee and Jokipii*, 1975; *Sato and Fehler*, 1998]. The wandering effect is derived from the parabolic wave equation within the Markov approximation. It is given by *Sato and Fehler* [1998] as

$$w(r,t) = \frac{v_0}{\sqrt{2\pi A(0) r}} \exp\left(-\frac{v_0^2 r^2}{2A(0)r}\right), \qquad (29)$$

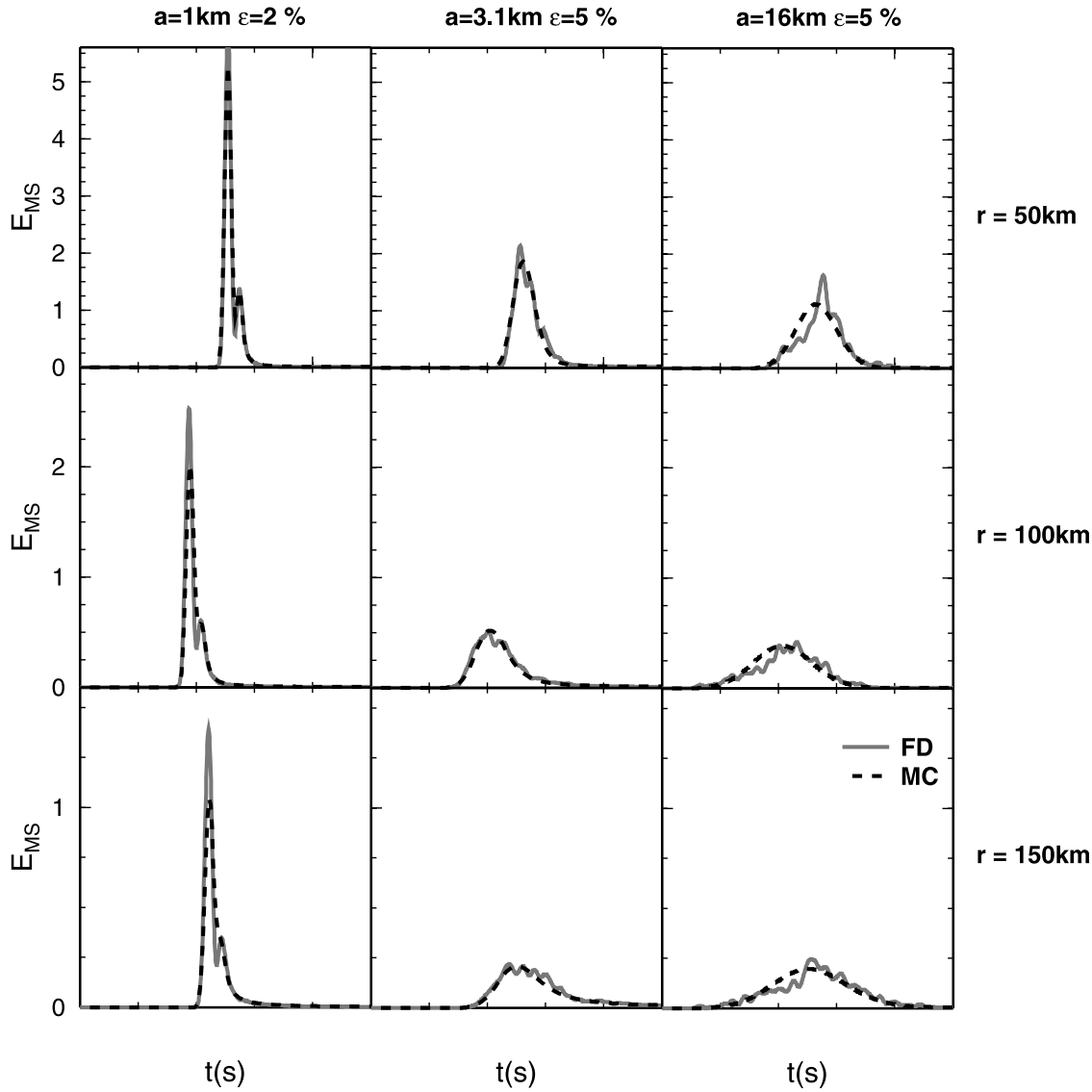

Figure 11. Direct energy pulses for an exponential medium convolved with the wandering effect from (equation (29)). The agreement of directly pulses between FD and MC gets better compared with Figure 9.

where r is the propagation distance, v_0 is the mean velocity and A is the longitudinal integral of the ACF [*Sato and Fehler*, 1998]:

$$A(x=0,z) \equiv \int_0^\infty P(x=0,z)dz = \begin{cases} \sqrt{\pi}\varepsilon^2 a & \text{Gaussian,} \\ 2\varepsilon^2 a & \text{Exponential,} \end{cases} \tag{30}$$

where z is the direction of propagation. In Figures 11 and 12, $w(r, t)$ is used as an additional convolution operator for the MC envelopes. Shape and amplitude of the envelope around the first arrival now agree very well between MC and FD even for large ak. This result is remarkable, as the MC solution using the angle-dependent single scattering coefficients provides a tool to simulate envelopes of whole wave trains in randomly fluctuating media from the first P arrival until the late coda, if the wandering effect is taken into account additionally. The wandering effect is not part of RTT and is applied here to P wave energy only, but could be extended to arbitrary particle paths by counting P and S path lengths separately and applying the appropriate convolution to the time function of each particle separately.

6. Discussion and Conclusion

[14] We developed a Monte Carlo scheme for the simulation of MS vector wave envelopes in 2-D random elastic media. It is based on the radiative transfer theory, where the individual scattering processes are described by angular-dependent Born scattering coefficients. The simulated envelopes have been compared to average envelopes derived from full wavefield simulations with a finite difference method for a broad range of correlation lengths and for Gaussian and exponential ACFs. Our general result is that the Monte Carlo solution yields surprisingly accurate envelope

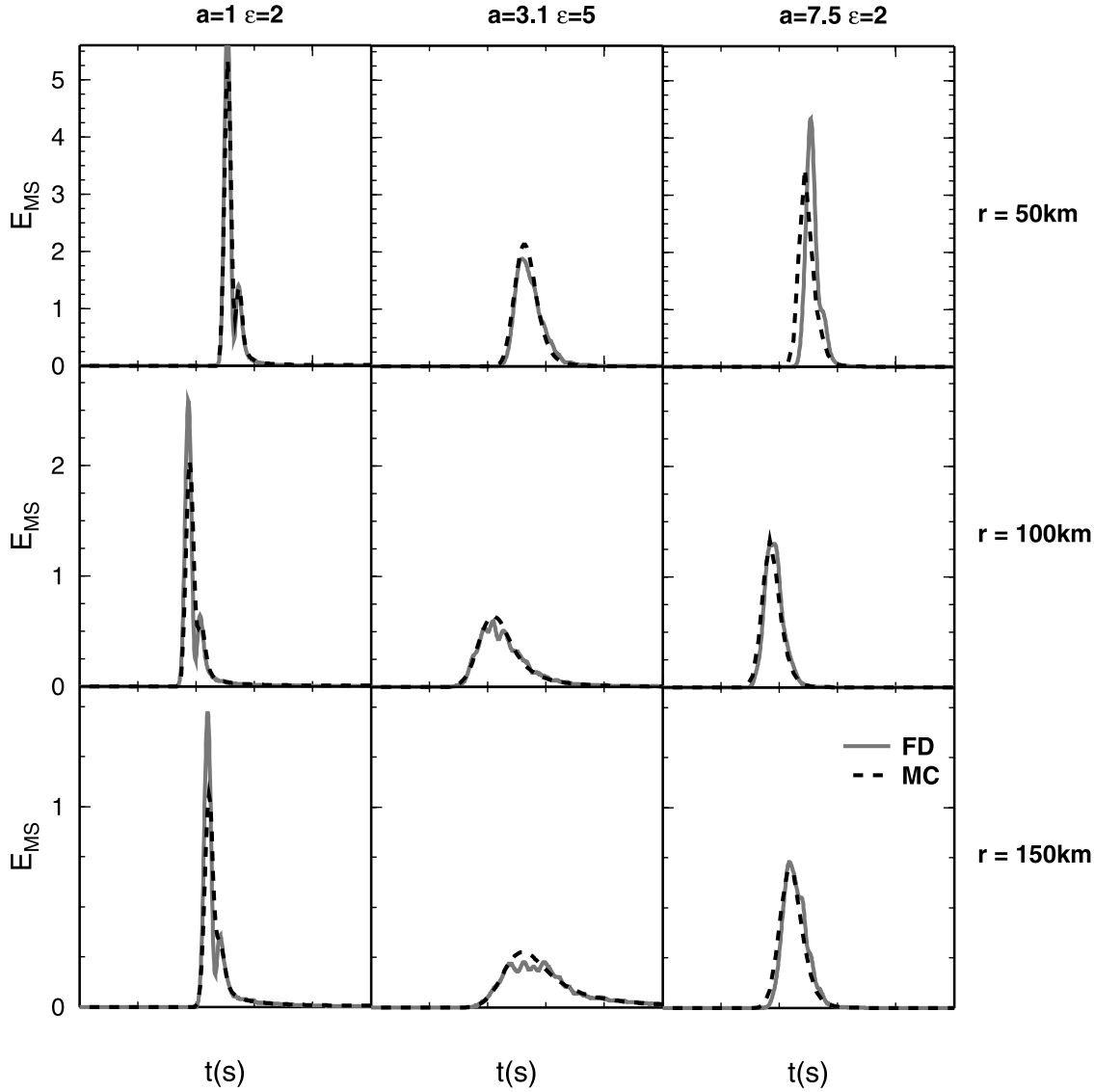

Figure 12. Same as Figure 11 for a Gaussian medium convolved with the wandering effect (equation (29)).

shapes not only for the late coda, but also for the time range of the initial *P* and *S* wave arrival, i.e., forward or small angle scattering, in the strong forward scattering regime $ak \gg 1$. This is surprising, as it is predicted from theoretical considerations that radiative transfer breaks down in these cases. For the acoustic case, *Wegler et al.* [2006] found similar results by comparing RTT with Markov approximation and FD simulations.

[15] RTT cannot explain the pulse broadening occurring for $ak \gg 1$ caused by traveltime fluctuations of individual ray paths through the random medium which is present in the FD stacks. However, this broadening is well described by the wandering effect which is given analytically, and can be easily included by convolving the MC envelopes with the appropriate filter function. Moreover, this effect only appears in data, if an envelope stack is done without first correcting for traveltime fluctuations of the individual traces. If the traces are aligned to the first onset before stacking, the wandering effect will disappear. Only for Gaussian ACF, weak perturbation and strong forward scattering a discrepancy occurs between RTT and FD. We speculate that this could be caused by near field terms which are neglected in the Born approximation, but are responsible for conversion scattering observed in the FD simulations. We also find that in this case the coda level may be very sensitive to small changes in frequency.

[16] Because of the expected breakdown of Born approximation for $ak \gg 1$, *Sato et al.* [2004] proposed a hybrid method for acoustic waves, where the Born scattering coefficients are replaced by so-called momentum transfer scattering coefficients which exclude the near forward direction and replace the large angle part by some effective isotropic scattering coefficient. Forward scattered waves are then modeled by a Markov propagator. Our results show that it does not seem to be necessary to model early and late coda parts with different analytical or numerical approaches, but that the use of angular-dependent Born coefficients in RTT offers a unified approach. However, a disadvantage of our version of RTT in the strong forward scattering regime is that the mean free path length becomes very small.

Therefore many scattering interactions have to be computed, but each time the particle is scattered close to the forward direction and therefore effectively follows an almost straight ray path. This multiple scattering increases computing time substantially. One may think of clever algorithms that replace a whole sequence of forward scattering events with an increase of mean free path length.

[17] Here, we restricted ourselves to the 2-D case, because our aim was to validate the envelope simulation method against full solutions of the elastic equations. FD methods for three dimensions are available, but are still very cumbersome to use on most computers. We do not expect, however, that going to three dimensions will change our results significantly. One of the advantages of the MC method is that it is flexible. It is straightforward to implement variable background velocities, anisotropic source radiation patterns and reflection/transmission at discontinuities. We therefore conclude that the method has the potential of modeling envelopes in arbitrarily complex elastic media.

[18] **Acknowledgments.** This work was supported by Deutsche Forschungsgemeinschaft, under contract KO1068/5. We thank Haruo Sato for many stimulating discussions.

References

Aki, K. (1969), Analysis of the seismic coda of local earthquakes as scattered waves, *J. Geophys. Res.*, *74*(2), 615–631.

Aki, K., and B. Chouet (1975), Origin of coda waves: source, attenuation, and scattering effects, *J. Geophys. Res.*, *80*(23), 3322–3342.

Apresyan, L., and Y. A. Kravtsov (1996), *Radiation Transfer: Statistical and Wave Aspects*, Gordon and Breach, New York.

Bal, G., and M. Moscoso (2000), Polarization effects of seismic waves on the basis of radiative transport theory, *Geophys. J. Int.*, *142*, 571–585.

Bal, G., G. Papanicolaou, and L. Ryzhik (2000), Probabilistic theory of transport processes with polarization, *SIAM J. Appl. Math.*, *60*, 1639–1666.

Birch, A. F. (1961), The velocity of compressional waves in rocks to 10 kilobars, part 2, *J. Geophys. Res.*, *66*(7), 2199–2224.

Chandrasekhar, S. (1960), *Radiative Transfer*, Dover, Mineola, N. Y.

Dainty, A. M., and M. N. Toksöz (1977), Elastic wave propagation in a highly scattering medium—A diffusion approach, *J. Geophys. Res.*, *43*(1–2), 375–388.

Frankel, A., and L. Wennerberg (1987), Energy-flux model of seismic coda: Seperation of scattering and intrinsic attenuation, *Bull. Seismol. Soc. Am.*, *77*, 1223–1251.

Gusev, A. A., and I. R. Abubakirov (1987), Monte-Carlo simulation of record envelope of a near earthquake, *Phys. Earth Planet. Inter.*, *49*(1–2), 30–36.

Gusev, A. A., and I. R. Abubakirov (1999), Vertical profile of effective turbidity reconstructed from broadening of incoherent body-wave pulses - i. General approach and the inversion procedure, *Geophys. J. Int.*, *136*(2), 295–308.

Hoshiba, M. (1991), Simulation of multiple-scattered coda wave excitation based on the energy conservation law, *Phys. Earth Planet. Inter.*, *67*(1–2), 123–136.

Hoshiba, M. (1995), Estimation of nonisotropic scattering in western Japan using coda wave envelopes: Application of a multiple nonisotropic scattering model, *J. Geophys. Res.*, *100*(B1), 645–657.

Korn, M. (1993), Determination of site-dependent scattering *Q* from *P*-wave coda analysis with an energy-flux model, *Geophys. J. Int.*, *113*, 54–72.

Korn, M., and H. Sato (2005), Synthesis of plane vector wave envelopes in two-dimensional random elastic media based on the Markov approximation and comparison with finite-difference simulations, *Geophys. J. Int.*, *161*, 839–848.

Lee, L. C., and J. R. Jokipii (1975), Strong scintillations in astrophysics. ii. A theory of temporal broadening of pulses, *Astrophys. J.*, 201.

Levander, A. R. (1988), Fourth-order finite-difference *P-SV* seismograms, *Geophysics*, *53*, 1425–1436.

Lux, I., and L. Koblinger (1991), *Monte Carlo Particle Transport Methods: Neutron and Photon Calculations*, CRC Press, Boca Raton, Fla.

Margerin, L., M. Campillo, and B. A. Van Tiggelen (1998), Radiative transfer and diffusion of waves in a layered medium: New insight into coda *Q*, *Geophys. J. Int.*, *134*, 596–612.

Margerin, L., M. Campillo, and B. Van Tiggelen (2000), Monte Carlo simulation of multiple scattering of elastic waves, *J. Geophys. Res.*, *105*(B4), 7873–7892.

Müller, T. M., and S. A. Shapiro (2001), Most probable seismic pulses in single realizations of two and three dimensional random media, *Geophys. J. Int.*, *144*(1), 83–95.

Paasschens, J. C. J. (1997), Solution of the time-dependent Boltzman equation, *Phys. Rev. E*, *56*(1), 1135–1142.

Reynolds, A. C. (1978), Boundary conditions for the numerical solution of wave propagation problems, *Geophysics*, *43*, 1099–1110.

Rytov, S. M., Y. A. Kravtsov, and V. I. Tatarskii (1987), *Principles of Statistical Radiophysics*, vol. 4, *Wave Propagation Through Random Media*, Springer, New York.

Ryzhik, L., G. Papanicolaou, and J. B. Keller (1996), Transport equations for elastic and other waves in random media, *Wave Motion*, *24*, 327–370.

Saito, T., H. Sato, and M. Ohtake (2002), Envelope broadening of spherically outgoing waves in three-dimensional random media having power law spectra, *J. Geophys. Res.*, *107*(B5), 2089, doi:10.1029/2001JB000264.

Saito, T., H. Sato, M. Fehler, and M. Ohtake (2003), Simulating the envelope of scalar waves in 2D random media having power-law spectra of velocity fluctuation, *Bull. Seismol. Soc. Am.*, *93*(1), 240–252.

Sato, H. (1977), Single isotropic scattering model including wave conversions: Simple theoretical model of the short period body wave propagation, *J. Phys. Earth*, *25*, 163–176.

Sato, H., and M. C. Fehler (1998), *Seismic Wave Propagation and Scattering in the Heterogeneous Earth*, Springer, New York.

Sato, H., M. Fehler, and T. Saito (2004), Hybrid synthesis of scalar wave envelopes in two-dimensional random media having rich short-wavelength spectra, *J. Geophys. Res.*, *109*, B06303, doi:10.1029/2003JB002673.

Scherbaum, F., and H. Sato (1991), Inversion of full seismogram envelopes based on the parabolic approximation: Estimation of randomness and attenuation in southeast Honshu, Japan, *J. Geophys. Res.*, *96*(B2), 2223–2232.

Shearer, P. M., and P. S. Earle (2004), The global short-period wavefield modelled with a Monte Carlo seismic phonon method, *Geophys. J. Int.*, *158*, 1103–1117.

Trègourés, N. P., and B. A. van Tiggelen (2002), Generalized diffusion equation for multiple scattered elastic waves, *Waves Random Media*, *12*, 21–38.

Weaver, R. L. (1990), Diffusivity of ultrasound in polycrystals, *J. Mech. Phys. Solids*, *38*(1), 55–86.

Wegler, U. (2004), Diffusion of seismic waves in a thick layer: Theory and application to Vesuvius volcano, *J. Geophys. Res.*, *109*, B07303, doi:10.1029/2004JB003048.

Wegler, U., M. Korn, and J. Przybilla (2006), Modeling full seismogram envelopes using radiative transfer theory with Born scattering coefficients, in *Advances in Studies of Heterogeneities in the Earth's Lithosphere, Keiiti Aki Volume II*, Springer, New York, in press.

Williamson, I. (1972), Pulse broadening due to multiple scattering in the interstellar medium, *Mon. Not. R. Astron. Soc.*, *157*, 55–71.

Wu, R. (1985), Multiple scattering and energy transfer of seismic waves: Separation of scattering effect from intrinsic attenuation: I. Theoretical modelling, *Geophys. J. R. Astron. Soc.*, *82*(1), 57–80.

Wu, R., and K. Aki (1985), Elastic wave scattering by a random medium and the small-scale inhomogeneities in the lithosphere, *J. Geophys. Res.*, *90*(B12), 10,261–10,273.

Yoshimoto, K. (2000), Monte Carlo simulation of seismogram envelopes in scattering media, *J. Geophys. Res.*, *105*(B3), 6153–6161.

Zeng, Y. (1993), Theory of scattered *P*- and *S*-wave energy in a random isotropic scattering medium, *Bull. Seismol. Soc. Am.*, *83*(4), 1264–1976.

Zeng, Y., F. Su, and K. Aki (1991), Scattering wave energy propagation in a random isotropic scattering medium: 1. Theory, *J. Geophys. Res.*, *96*(B1), 607–619.

M. Korn, J. Przybilla, and U. Wegler, Institut für Geophysik und Geologie, Universität Leipzig, Talstraße 35, D-04103 Leipzig, Germany. (jprzybill@web.de)